Superconductor Science and Technology

PAPER

# Initial growth of tin on niobium for vapor diffusion coating of $Nb_3Sn$



IOP Publishing Superconductor Science and Technology
Supercond. Sci. Technol. 32 (2019) 045008 (18pp) https://doi.org/10.1088/1361-6668/aafa88

# Initial growth of tin on niobium for vapor diffusion coating of $Nb_3Sn$

**Uttar Pudasaini[1], Grigory V Eremeev[2], Charles E Reece[2], James Tuggle[3] and Michael J Kelley[1,2,3,4]**

[1] Applied Science Department, The College of William and Mary, Williamsburg, VA 23185, United States of America
[2] Thomas Jefferson National Accelerator Facility, Newport News, VA 23606, United States of America
[3] Virginia Polytechnic Institute and State University, Blacksburg, VA 24061, United States of America

E-mail: MJKell@wm.edu

Received 7 June 2018, revised 11 October 2018
Accepted for publication 21 December 2018
Published 1 March 2019

**Abstract**

$Nb_3Sn$ offers significant potential to exceed the performance of niobium for superconducting radio frequency accelerator cavities. The most promising path toward deployment is by tin vapor diffusion coating of Nb cavity interiors via a two step nucleation-then-growth sequence. Reported here is a materials science study of the nucleation process. We manipulated the accessible range of process variables and determined the effect on composition and microstructure using an array of materials characterization tools. Broadly, nucleation deposits tin as a thin surface phase and, under some conditions, as near-micron sized particles as well, resembling Stranski–Krastanov growth. Conditions that impair nucleation promote the formation of defects, such as patches, in subsequent coating growth. Otherwise no significant effect on the subsequently grown coating was found for structures produced during nucleation.

Keywords: $Nb_3Sn$, nucleation, SRF cavity, vapor diffusion coating, Stranski–Krastanov growth

(Some figures may appear in colour only in the online journal)

## 1. Introduction

Modern particle accelerators use superconducting radio frequency (SRF) cavities to accelerate a beam of charged particles. Niobium has been the material of choice so far to fabricate SRF cavities. However, their operation is very expensive as they need to maintain a ~2 K cryogenic temperature for effective operation. Further, after more than five decades of research, the performance of niobium cavities is approaching the theoretical limit set by intrinsic material properties. Application of new materials instead can improve the performance as well as reduce the cost of SRF accelerators [1].

Discovered in 1954 by Bernd Matthias [2], $Nb_3Sn$ is a promising alternative. Its critical temperature (~18 K) and predicted superheating field (~400 mT) are nearly twice those of niobium, thereby offering the possibility of attaining higher quality factor and accelerating gradient at any given temperature [3]. It can also allow an increase of the cavity operation temperature, resulting in significant reduction in both capital and operating cost for the cryoplant. However, $Nb_3Sn$ is a challenging material for cavity application because of lower thermal conductivity and brittleness. That restricts its application to coating form. SRF cavities typically have complicated geometries that need to be coated uniformly, which limits the coating techniques available.

Several techniques have been attempted to deposit $Nb_3Sn$ layers: chemical vapor deposition, co-evaporation, tin bath dipping and annealing, pulsed laser deposition, electro-deposition, sputtering etc [4–11]. However, vapor diffusion coating of $Nb_3Sn$, attributed to Saur and Wurm [12], is the most favorable and successful technique so far. Preparation of $Nb_3Sn$ cavities by diffusion coating on niobium cavities dates back to the 1970s [13–15]. Several research institutions working currently to develop $Nb_3Sn$ coated cavities use it [16–18]. Recent performance results of such cavities are very promising, attaining quality factor $>10^{10}$ operating at 4.2 K with gradient more than 15 MV $m^{-1}$ [19, 20]. The essence of the process is to transport tin vapor to the niobium substrate, and provide the high

[4] Author to whom any correspondence should be addressed.

 

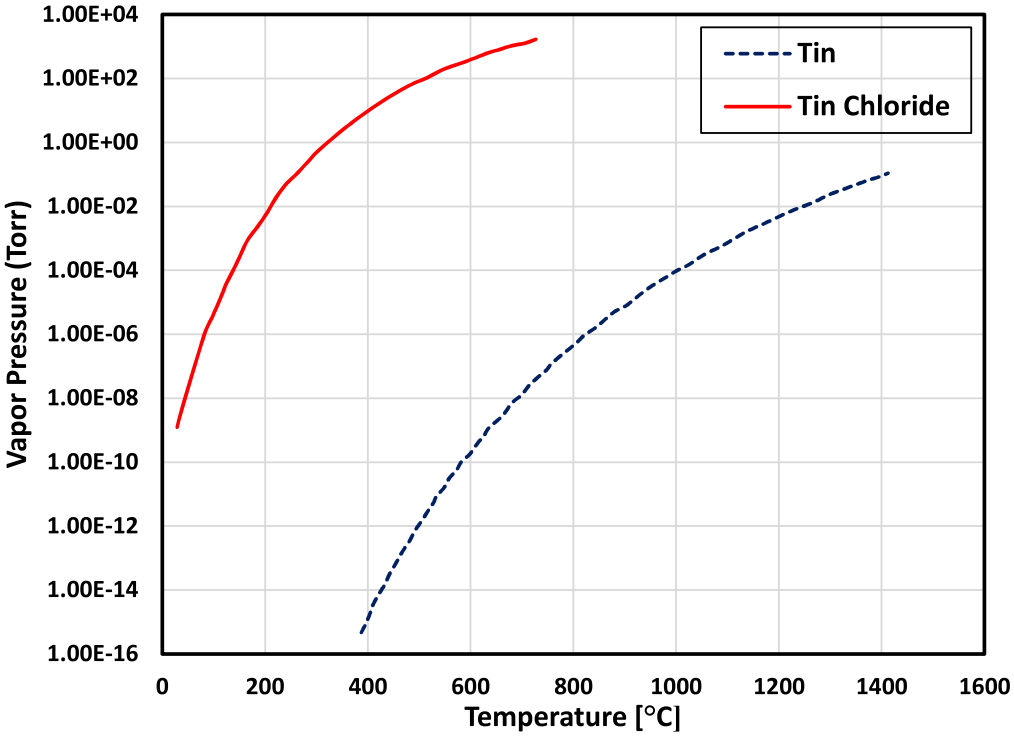


**Figure 1.** Vapor pressure of tin and tin chloride. Reproduced with permission from [24], which cites [25–27].

temperature environment, >930 °C, to form the $Nb_3Sn$ phase exclusively, which is determined by the binary phase diagram [21]. Early attempts at Siemens AG with this method resulted in regions which were not covered completely with $Nb_3Sn$ [22]. The proposed cause was irregular nucleation. They prescribed to anodize the Nb-substrate prior to coating while setting the temperature of tin source higher than the substrate temperature, which they believed enhances nucleation by increasing the tin vapor supply. Another solution was to add a small amount of Sn halide which can decompose to yield an increased Sn supply at lower temperature. The idea was adopted with expected benefit from the higher vapor pressure of tin halide than elemental tin [23]. For example, comparison of Sn vapor pressure to $SnCl_2$ vapor pressure is shown in figure 1. $SnCl_2$ evaporates at temperature of about 500 °C to deposit tin sites on the niobium surface, which were assumed to act as Nb–Sn nucleation sites.

Research institutions following a similar $Nb_3Sn$ coating recipe later preferred $SnCl_2$, combined sometimes with substrate preanodization or adjusting a temperature gradient between the tin source and the niobium substrate. Later studies suggested that substrate preanodization is not mandatory, and it also results in residual resistivity ratio (RRR) degradation due to oxygen absorption from the anodic layer [28]. Application of Sn halide is especially helpful for the coating systems that do not have a secondary heater to set up a temperature gradient between the Sn source and the substrate, as discussed above.

Figure 2 depicts a typical $Nb_3Sn$ coating process at JLab. The first temperature plateau at 500 °C is dedicated to the nucleation process and the second at 1200 °C facilitates coating growth.

While the inclusion of a nucleation step has a long history, only limited research has been done to understand the fundamental atomic process or its relevance and effect on the resulting coating. The purpose of this work was to gain more insight into the nucleation step.

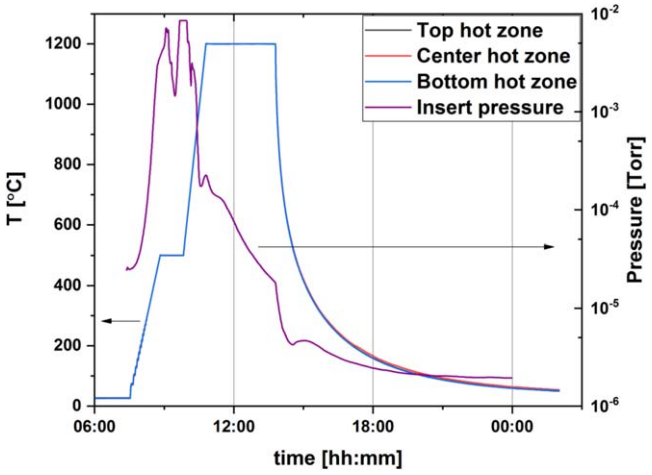


**Figure 2.** Temperature profile used for coating $Nb_3Sn$ on niobium samples at JLab. Temperature of the insert during the process is monitored with three thermocouples at different sections of the insert. Because of very similar temperature readings, the temperature curves are overlapped.

## 2. Experimental description

### *2.1. Materials*

The samples studied here were 10 mm × 10 mm coupons of fine grain niobium, prepared by electrical discharge machining


**Figure 3.** Sample chamber, samples, tin and tin chloride packages, and niobium foils before set up. Insert is not shown.

cutting from 3 or 4 mm thick, high RRR ($\sim$ 300) sheet material of the type used to fabricate SRF cavities. All samples were subjected to buffered chemical polishing (BCP) using a solution of 49% HF, 70% $HNO_3$ and 85% $H_3PO_4$ in the ratio of 1:1:1 by volume with minimum removal of 50 $\mu$m. These samples received further metallographic polishing, also known as nanopolishing (NP), which typically removes $>100$ $\mu$m and produces smoother surfaces favorable to most material characterization techniques. 'Nanopolishing' is term applied to chemomechanical planarization technology developed in the microelectronics industry. While the specifics are proprietary and closely-held, polishing with silica or alumina slurries with unidentified additives and modifiers is understood to be central.

The average roughness of NP samples was below 5 nm as measured from 50 $\mu$m $\times$ 50 $\mu$m area scans using atomic force microscopy (AFM) [29].

### 2.2. Experimental setup

The coating growth system is comprised of two parts: the furnace to provide a clean heating environment and the insert, made of niobium, within which the experimental setup is loaded for each experiment. The temperature was monitored using three thermocouples outside the insert. A detailed description of the coating growth system can be found in [18].

The insert houses a sample chamber made of niobium with a shelf to mount coupon samples inside, figure 3. One gram of 99.999% or better purity tin shots ($\sim$3 mg cm$^{-2}$ of surface to be coated) and the chosen amount of 99.99% tin chloride powder, both purchased from American Elements, were packaged loosely in niobium foil, and placed on the niobium plate/foil which covered the bottom end of sample chamber. The amount of tin chloride was varied in some experiments. Sn and $SnCl_2$ vapor are expected to exit from the package readily from the narrow openings. The top end was later covered by niobium plate/foil after mounting the experimental coupon samples inside. The sample chamber, samples, chemicals, and the covering foils/plates were assembled in the clean room to limit any contamination before installation into the coating growth system.

### 2.3. Experimental work flow

The experimental protocol consisted of loading the chosen amount of tin and tin chloride into the foil packages. The Nb samples were then placed on the sample chamber shelf visible in figure 3. See also the previous section. The top of the sample chamber was covered with Nb foil or a Nb plate and placed into the insert. The insert was closed and placed within the furnace, which was then closed. The entire system was pumped down until pressure in the insert attained the $\sim 10^{-5}$ Torr range before the heating profile was initiated. The temperature inside the insert was raised at the rate of 6 °C min$^{-1}$ until it reached the target nucleation temperatures as shown in table 1. These temperatures were maintained constant for different time periods (nucleation time) before ceasing the heating process. After the nucleation at given condition, the chamber was allowed to cool down in vacuum. After reaching room temperature, the insert was purged with nitrogen to regain atmospheric pressure. The sample chamber was then taken out to remove the nucleated samples.

**Table 1.** Nucleation experiments.

| Nucleation temperature | 300 °C | 400 °C | 450 °C | 500 °C |
|---|---|---|---|---|
| Nucleation time | 1–4 h | 1 h | 1 h | 5 min–5 h |
| Amount of $SnCl_2$ | 1 g | 1 g | 1 g | 5 mg, 1 g |
| Amount of Sn | 1 g | 1 g | 1 g | 0 g, 1 g |

A selected few experiments also featured pre-anodized niobium samples along with regular niobium samples. Following the examination of nucleated samples, a set of different nucleation profiles were employed to grow the complete $Nb_3Sn$ coatings by a further coating step as shown in figure 2. Other experiments included interruption of the process at different stages with/without nucleation to further understand its effect in subsequent coating.

### *2.4. Characterization*

A basic premise of materials science is that structure (composition, topography, ...) determines properties. SRF cavity materials have not attracted broad attention in the materials characterization community, so a consensus approach has not yet developed. We seek to take steps in that direction by applying a number of well-established techniques in this initial phase of our research program, deferring novel and emerging techniques to the future. Probably the most familiar technique of all is scanning electron microscopy with elemental analysis. An Hitachi 4700 field emission scanning electron microscope (FE-SEM) equipped with an energy dispersive x-ray spectroscopy (EDS) detector was used to examine the nucleated samples. SEM images were taken after each experiment, and elemental composition was analyzed with EDS. All SEM images were taken at 0° tilt angle, using a 12/15 kV accelerating voltage. Under ideal conditions, SEM/EDS can measure element concentration down to approximately 0.1 atomic percent. As the primary beam enters the specimen, electrons lose energy so that they reach a limited depth while retaining enough energy to cause x-ray emission. The Castaing approximation permits estimation leading to values of 0.84 $\mu$m for Nb and 0.98 $\mu$m for Sn with a 15 kV primary beam energy. The electrons are also deflected outside the original beam path, so that lateral resolution decreases.

The topographic examination used a Digital Instruments IV AFM in tapping mode with aluminum reflex coated silicon tips with radius $<$10 nm, resonant frequency 190 KHz and force constant 48 N m$^{-1}$. The selected samples were scanned for 5 $\mu$m $\times$ 5 $\mu$m and 1 $\mu$m $\times$ 1 $\mu$m sizes with 512 $\times$ 512 data points. The expected lateral resolution of AFM is defined by the spacing of sampling points. For example, the expected lateral resolution for 5 $\mu$m scan is 5 $\mu$m/512 ($\sim$10 nm) at optimal conditions.

Surface sensitive elemental analysis was done using x-ray photoelectron spectroscopy (XPS), probing the elemental composition of the first few nanometers of surfaces down to concentration of approximately 0.1 atomic percent. The XPS measurements were carried out in an ULVAC-PHI 'Quantera SXM' instrument equipped with a monochromated Al K$\alpha$ x-ray source. Spectra were collected at 50 W/15 kV using a 200 $\mu$m spot size, 45° take off angle.

Scanning Auger microscopy (SAM) using a PHI 680 system was employed for certain samples. It consists of a FE-SEM with a Schottky emission cathode, a secondary electron detector, and an axial cylindrical mirror analyzer with a multi-channel detector to collect Auger electrons produced during electron imaging. Very small spot sizes can be realized with this instrument, down to 7 nm.

Transmission electron microscopy (TEM) imaging of the cross-section of a nucleated sample was carried out using a JEOL 2100 operating at 200 kV. The specimen was prepared by focused ion beam (FIB, Helios Nano Lab 600) sectioning using the lift-out technique. In order to preserve the surface of nucleated sample and create an intact cross-section, a protective layer of Pt was deposited on the sample surface over the area of interest prior sectioning. Initial material removal steps were performed at the highest removal rate of 30 kV. The final polishing step was done with 2 kV Ga ions at an angle of 7°.

## 3. Results and discussion

### *3.1. Nucleation temperature variation*

Temperatures of 300 °C, 400 °C, 450 °C and 500 °C were chosen to study the effect of nucleation temperature. Since the vapor pressure of $SnCl_2$ drops rapidly below 300 °C, see figure 1, this was chosen as the lower bound of the studied temperature range. The treatment time was kept constant at one hour, and the amount of $SnCl_2$ was fixed to 1 g. Residual $SnCl_2$ was found inside the niobium foil containing supplied $SnCl_2$, only after 300 °C and 400 °C.

Variation in parameters in those treatments resulted in different surface features. After 300 °C nucleation, a significant portion of $SnCl_2$ was found inside each package. SEM images revealed nanometer-sized particles, assumed to be tin, on the niobium surface, figure 4(a). However, only niobium was detected with EDS, possibly due to the shallow coverage of very small amount of deposited tin. The nucleation temperature of 400 °C produced distinct features on the surface, figure 4(b). Besides micron sized spherical particles, extended interconnected 'mud-crack' like features were seen in SEM images. Several SEM images, not shown here, inferred that the big particles were formed by the accumulation of those features. Both niobium and tin signals were detected with EDS not only at the spherical particles, which we assume are tin, but also between the particles, where the irregular structures can be seen in SEM image.

Nucleation temperatures of 450 °C and 500 °C created similar looking surfaces with sub-micron sized spherical particles visible in the SEM, appearing as bright features in figures 4(c) and (d). The size and distribution of the particles was slightly varied between these two temperatures. Spherical particles were examined with EDS, showed 40–70 at% Sn depending on size. Larger particles showed more tin, as would be expected, since the spatial resolution limit of EDS is larger than the particle size. Therefore the data from

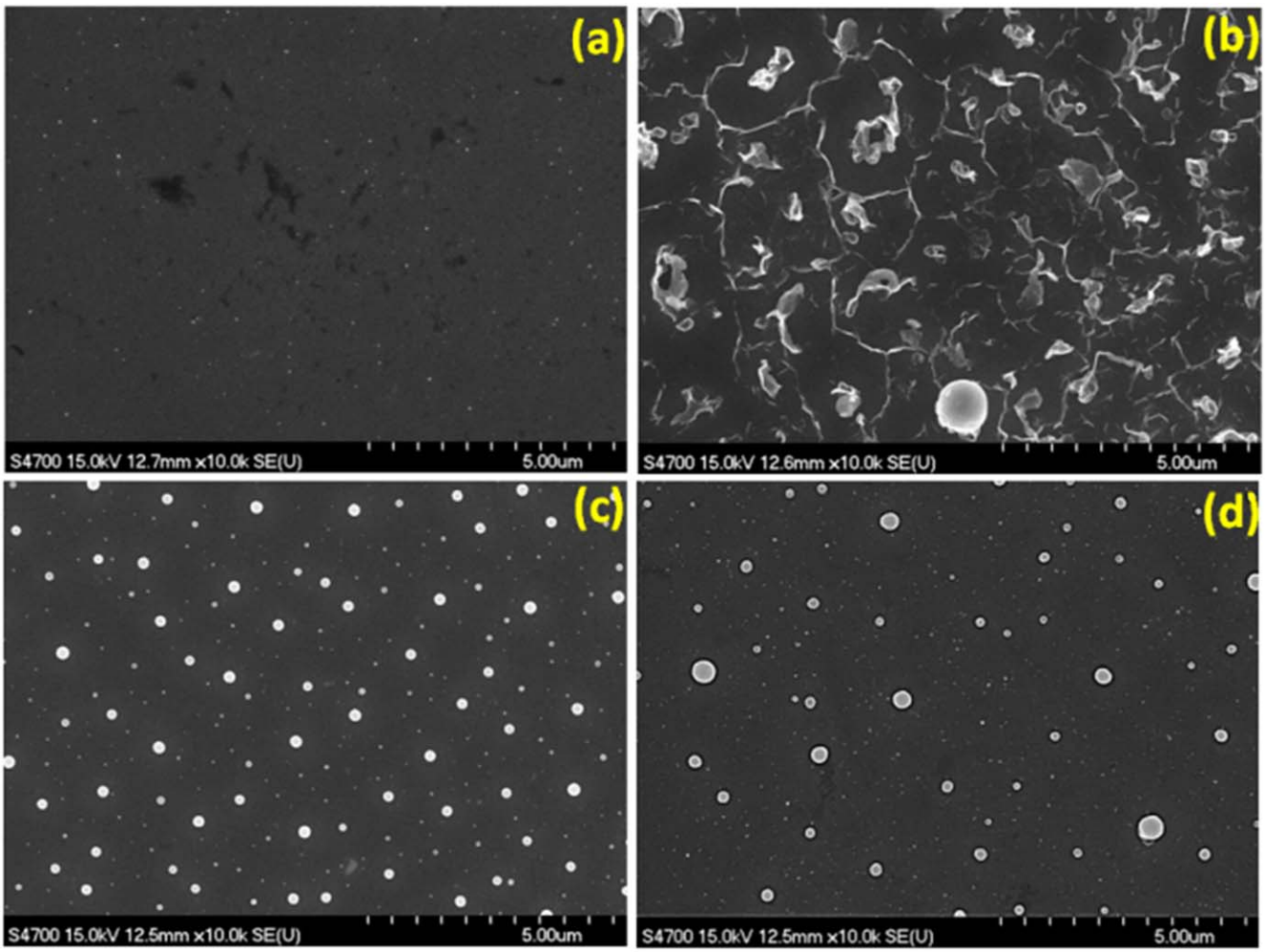


**Figure 4.** SEM images obtained from samples activated at nucleation temperature of (a) 300 °C, (b) 400 °C, (c) 450 °C, and (d) 500 °C with constant nucleation time of an hour. Circular bright features are tin particles when examined with EDS. Reproduced from [30]. CC BY 3.0.

**Table 2.** XPS elemental analysis of nucleated samples at different temperature. Nucleation time for each sample was one hour.

| Nucleation temperature (°C) | Sample | C (at%) | O (at%) | Nb (at%) | Sn (at%) | $\frac{Sn}{Nb+Sn} \times 100$ | |
|---|---|---|---|---|---|---|---|
| 300 | U55 | 48.5 | 32.5 | 13.7 | 5.3 | 27.89 | |
| | | 6.1 | 61.5 | 28.5 | 3.9 | 12.03 | With pre-sputtering |
| 400 | U73 | 35.0 | 41.5 | 9.4 | 14.1 | 60.00 | |
| | | 4.9 | 57.8 | 25.1 | 12.2 | 32.71 | With pre-sputtering |
| 450 | U59 | 62.5 | 25.5 | 5.7 | 6.3 | 52.5 | |
| | U47 | 9.0 | 54.2 | 28.6 | 8.2 | 22.28 | With pre-sputtering |
| 500 | U90 | 56.8 | 31.2 | 7.3 | 4.7 | 39.17 | |
| | | 13.3 | 52.5 | 25.3 | 8.9 | 26.02 | With pre-sputtering |

individual particles included more or less Nb signal as well from adjacent or underlying material. EDS was unable to detect any tin in between those particles.

Samples from each experiment were examined using XPS (table 2). Carbon and oxygen were found, which is expected from post-experiment exposure to ambient atmosphere. The samples were then sputtered lightly (1 kV Ar, 30 s) to reduce the contaminants' contribution and scanned again. Pre-sputtering resulted in increased amount of oxygen, and reduced carbon in each XPS analysis. Removing the carbon increased the ratio of Nb to Sn, raising the possibility that tin may be present as a very thin surface layer, which was slightly sputtered. Alternatively, tin may have been preferentially sputtered compared to niobium. The tin and niobium were present only as an oxide. The data obtained from samples with nucleation temperature above 400 °C showed 20%–30% total tin. A typical XPS scan is shown in figure 5. Note the absence of chlorine peaks: no chlorine was ever found in any of the nucleated samples.

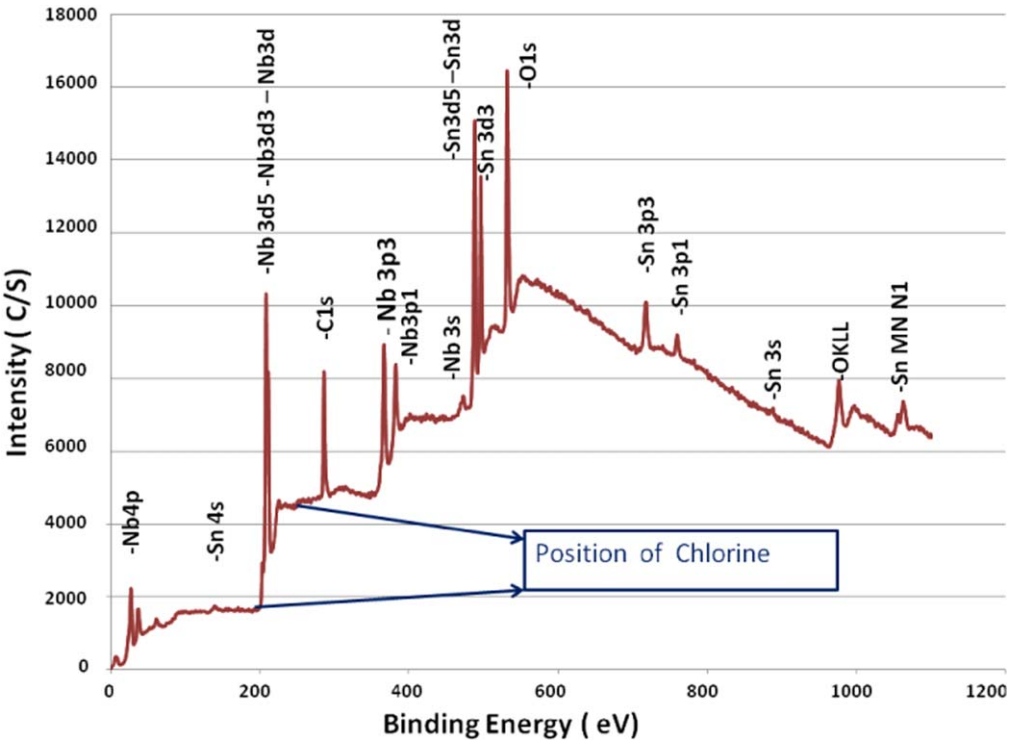


**Figure 5.** XPS data obtained from a sample after one hour at 500 °C.

**Table 3.** Calculated fractional surface coverages.

| Condition | 1 h at 500 °C | 1 h at 450 °C | 4 h at 500 °C (section 3.2) | 5 h at 500 °C (section 3.3) |
|---|---|---|---|---|
| Coverage by particles (%) | 2.8 ± 0.6 | 3.9 ± 0.6 | 10.0 ± 0.8 | 1.9 ± 0.4 |

The amount of tin found with XPS on the surface is clearly more than expected from the very low surface coverage (table 3) by tin particles alone.

This discrepancy of tin content between SEM and XPS analysis indicated the presence of more tin than the particles visible in SEM. To gain insight into the form of tin on the surface, we adopted a model for calculation, consisting of the visible particles and a thin surface layer. The particles are treated as pure tin hemispheres, consistent with the SEM images and the AFM results presented later. The tin signal comes only from the surface of the particle. The surface layer is treated as a pure tin film, one atomic layer thick. The layer is too thin to be revealed with SEM/EDS, but can be detected by XPS. A rough intensity ratio of Sn/Nb in XPS was then estimated considering a homogeneous Sn layer of monoatomic thickness in between tin particles on the niobium surface. For the case when there is a thin layer of Sn on top of bulk niobium, the layer and substrate intensities are given by [31],

$$I_{\mathrm{Sn}} = I_{\mathrm{Sn}}^{\infty}\left[1 - \exp\left(-\frac{d}{\lambda_{\mathrm{Sn,Sn}}\cos\theta}\right)\right] \tag{1}$$

$$I_{\mathrm{Nb}} = I_{\mathrm{Nb}}^{\infty}\exp\left(-\frac{d}{\lambda_{\mathrm{Nb,Sn}}\cos\theta}\right), \tag{2}$$

where $I_{\mathrm{Sn}}^{\infty}$ and $I_{\mathrm{Nb}}^{\infty}$ are the intensities of the pure bulk tin and niobium. $\lambda_{\mathrm{Sn,Sn}}$ and $\lambda_{\mathrm{Nb,Sn}}$ are the attenuation length (inelastic mean free path) of the electrons in tin emitted by first subscript element to second subscript element. Emission angle, $\theta$ is the angle between the surface normal and direction of measured electron emission.

Dividing equation (1) by (2),

$$\frac{I_{\mathrm{Sn}}}{I_{\mathrm{Nb}}} = \frac{I_{\mathrm{Sn}}^{\infty}\left[1 - \exp\left(-\frac{d}{\lambda_{\mathrm{Sn,Sn}}\cos\theta}\right)\right]}{I_{\mathrm{Nb}}^{\infty}\exp\left(-\frac{d}{\lambda_{\mathrm{Nb,Sn}}\cos\theta}\right)}. \tag{3}$$

The intensity ratio of bulk tin and niobium is given by [32],

$$\frac{I_{\mathrm{Sn}}^{\infty}}{I_{\mathrm{Nb}}^{\infty}} = \frac{\mathrm{N_{Sn}}\sigma_{\mathrm{Sn}}\lambda_{\mathrm{Sn}}T_{\mathrm{Sn}}}{\mathrm{N_{Nb}}\sigma_{\mathrm{Nb}}\lambda_{\mathrm{Nb}}T_{\mathrm{Nb}}}, \tag{4}$$

where $N$ is atomic density, $\sigma$ is photo-ionization cross-section for observed photoelectron line and $T$ is transmission factor of

**Table 4.** Model parameters.

| $N_{Sn}$ (atoms cm$^{-3}$) | $N_{Nb}$ (atoms cm$^{-3}$) | $\lambda_{Sn}$ for $3d_{5/2}$ (nm) | Monolayer thickness, $d$ (nm) |
|---|---|---|---|
| $3.708 \times 10^{22}$ | $5.555 \times 10^{22}$ | 2.316 nm | 0.290 nm |

**Table 5.** Ratio of Sn to (Nb + Sn) obtained from model calculation of dependence of intensity on emission angle.

| | Angle between the surface normal and direction of electron emission (degrees) | | | |
|---|---|---|---|---|
| Model | 30 | 45 | 60 | 75 |
| Monolayer only | 0.09 | 0.11 | 0.16 | 0.29 |
| With 3% particles | 0.12 | 0.14 | 0.18 | 0.31 |
| With 5% particles | 0.14 | 0.16 | 0.20 | 0.33 |
| With 10% particles | 0.18 | 0.20 | 0.24 | 0.36 |

**Table 6.** ARXPS ratio of Sn to (Nb + Sn).

| | Angle between the surface normal and direction of electron emission (degree) | | | |
|---|---|---|---|---|
| Samples | 30 | 45 | 60 | 75 |
| U101(~5 mg $SnCl_2$) | 0.15 | 0.15 | 0.14 | 0.12 |
| M46 (1 g $SnCl_2$) | 0.19 | 0.18 | 0.22 | 0.19 |
| U66 (~5 mg $SnCl_2$) | 0.31 | 0.35 | 0.42 | 0.50 |
| U90 (1 g $SnCl_2$) | 0.16 | 0.18 | 0.20 | 0.22 |

instrument. From (3) and (4),

$$\frac{\frac{I_{Sn}}{\sigma_{Sn}\lambda_{Sn}T_{Sn}}}{\frac{I_{Nb}}{N_{Nb}\sigma_{Nb}\lambda_{Nb}T_{Nb}}} = \frac{N_{Sn}\left[1 - \exp\left(-\frac{d}{\lambda_{Sn,Sn}\cos\theta}\right)\right]}{N_{Nb}\exp\left(-\frac{d}{\lambda_{Nb,Sn}\cos\theta}\right)}. \quad (5)$$

The ratio on the left-hand side gives the corrected intensity ratio $\eta$, that is, the ratio of tin to niobium,

$$\frac{\eta_{Sn}}{\eta_{Nb}} = \frac{N_{Sn}\left[1 - \exp\left(-\frac{d}{\lambda_{Sn,Sn}\cos\theta}\right)\right]}{N_{Nb}\exp\left(-\frac{d}{\lambda_{Nb,Sn}\cos\theta}\right)}. \quad (6)$$

Let us use $3d_{5/2}$ photoelectron line for calculation. For E (Al $K_\alpha$) = 1486.7 eV,

$$\text{K.E.}\,(3d_{5/2})_{Sn} = E(\text{Al}\,K_\alpha) - E_b = 1486.7 - 484.9 = 1001.8\ \text{eV}, \quad (7)$$

where K. E. ($3d_{5/2}$) and $E_b$ are the kinetic energy and binding energy of the emitted $3d_{5/2}$ photoelectron.

For simplicity, $\lambda_{Sn,Sn} = \lambda_{Nb,Sn} = \lambda_{Sn}$, which can be extracted from the NIST electron inelastic mean free path database [33], using the kinetic energy of emitted photoelectrons. The required parameters to calculate the ratio of tin to niobium in equation (6) are shown in table 4. $\theta = 45°$, the one used in XPS measurement was chosen.

Table 5 presents calculations for 0%, 3%, 5% and 10% coverage by tin particles thick enough to shield all the photoelectrons from underlying niobium. The representative Sn/(Sn + Nb) ratio for 10% surface coverage was found to be ~20%, obtained by taking the weighted average of contributions from Sn particles (10%) and monolayer of Sn on bulk Nb (90%). This ratio is consistent with Sn concentration range of XPS analysis above, which supports the notion of a thin Sn layer on nucleated surfaces.

To further corroborate the finding, angle resolved XPS (ARXPS) was attempted on a few samples. XPS data were collected by varying the angle between XPS detector and sample surfaces (table 6). XPS intensity from a thin film is expected to vary depending on the emission angle, since the angle changes the effective information depth, see equation (1). The shallower angles increase signal contribution from the thin film. ARXPS results are summarized in table 6. While all four samples were nucleated at 500 °C, M46 and U90 were subjected to standard protocol (1 h of nucleation time with 1 g of $SnCl_2$). Two other samples, U101 and U66 were prepared with 5 mg (~10 $\mu$g cm$^{-2}$) of $SnCl_2$ and 5 h of nucleation time. Detailed description of preparation and analysis of similar samples will be presented later.

The model calculations indicate that a continuous film is expected to give a tin ratio at 75° at least twice that at 30° for all particle coverages. Sample U66 is an example. A surface covered by separated nanoparticles (not the SEM visible particles) will show no such variation with angle, since the information depth is not changing with rotation. U101 and M46 offer examples. U90 evidences some measure of the expected angle dependence, but not to a degree that would support any firm conclusion. These and other results not shown indicate that the two-dimensional species on the surface after nucleation are rather variable.

To gain more insight, a few samples were examined with SAM. In SAM, a 10 kV primary electron beam bombards the sample surface producing Auger, secondary and backscattered electrons. Auger electrons are used to identify the elements present; secondary and backscattered electrons are used for imaging at the same time, thus providing opportunity for surface sensitive elemental mapping in a SEM image. Results from a sample nucleated at 500 °C for one hour are shown in figure 6. Large and small bright features are evident in the secondary electron image (top left). The large features (red box) are consistent with the tin particles seen in the SEM and show expectedly high tin content in the spectral scans (top right). The intervening area shows small bright features and the presence of tin, (blue scan) at a much lower level. Elemental mapping of Sn and Nb appears in the lower

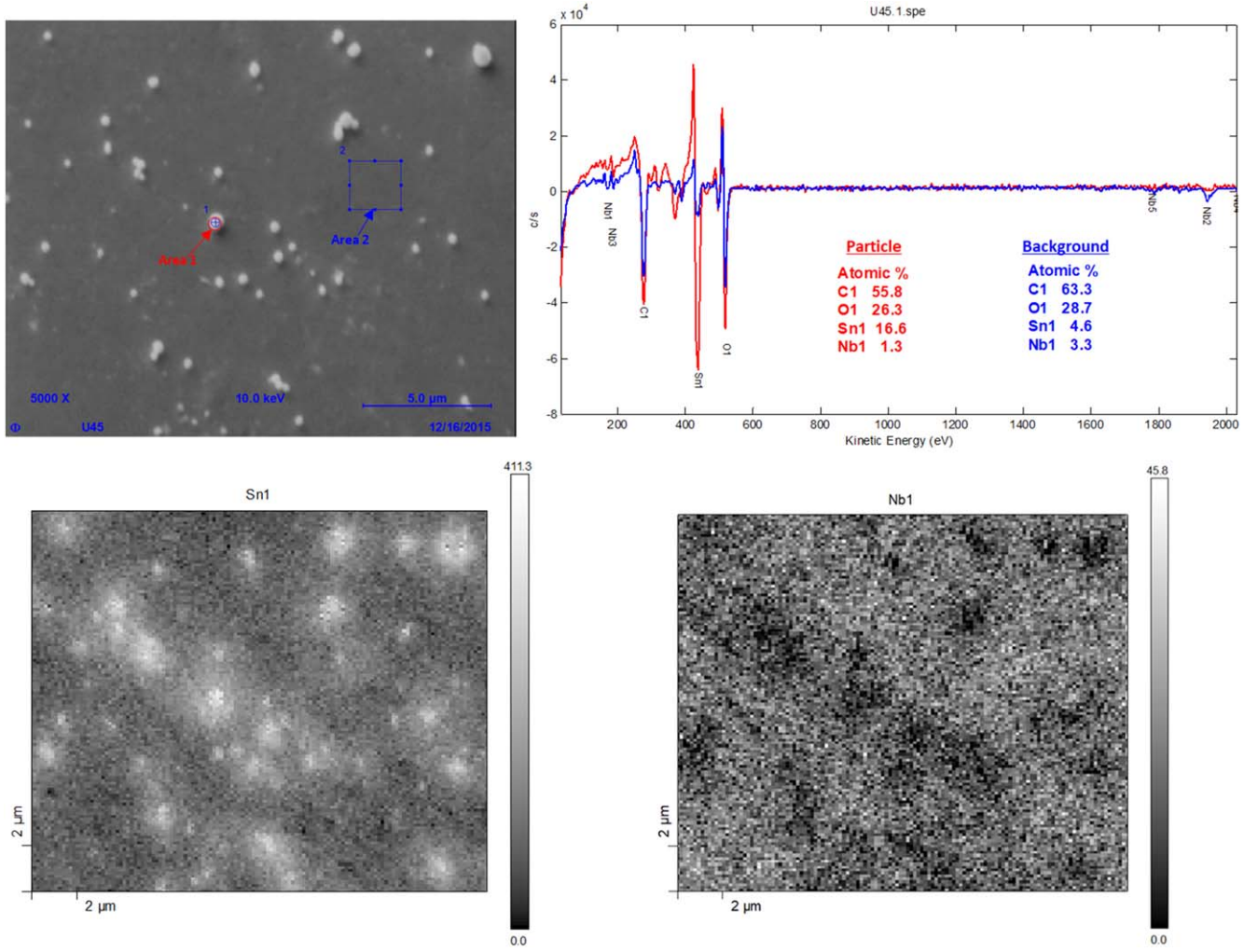


**Figure 6.** SAM elemental mapping of Sn coverage after sputtering for 30 s is shown in the image (lower left). The brighter areas are richer in Sn than darker area as shown by the intensity scale. Equivalent data for Nb appear at the lower right. Elemental composition comparison of particle and background is shown in spectra at the top right.

images. More investigation with a higher resolution instrument is needed to learn if these are an imaging artefact or tin nanoparticles.

TEM imaging of the cross-section of a nucleated sample, treated at 500 °C for 5 h was done. The sectioned area was chosen with SEM, and contained particles as well as areas away from particles, representing a usual nucleated sample. EDS line scans were obtained, passing through and away from the particles in the cross-section. An EDS line scan of an area away from tin particles (see figure 7) showed a brief jump of tin and oxygen signal close to the surface. This result is consistent with the previous finding of a tin surface layer by other characterization techniques discussed above.

An AFM image from a sample prepared under similar conditions, (figure 8(a)) showed the presence of tin particles as islands. More features (see area enclosed by rectangle in figure 8(a)) were seen in between tin islands. These features appeared following the nucleation; they are absent from a typical nanopolished sample. A height profile of a section from figure 8(a), passing through a big particle is shown in figure 8(b). The diameter of the largest particle in this scan was ∼200 nm with height of ∼60 nm. The largest particles observed were ∼300 nm in diameter.

The initial growth mode of thin films is commonly divided into three categories (Frank–Van Der Merve: two-dimensional (2D) layer growth; Stranski–Krastanov: layer plus three dimensional (3D) islands and Volmer–Weber: 3D island growth). Our data qualitatively resemble the Stranski–Krastanov mode; tin film is formed in addition to distributed tin particles. Similar growth has been reported before during the growth of tin on Al or Nb [34, 35]. The formation of a thin film, i.e., Frank–Van Der Merve growth, during nucleation was suggested from the early days of $Nb_3Sn$ diffusion coating [22, 36]. The growth of such continuous layer has been suggested to be crucial to establish uniform coating of $Nb_3Sn$. The role of $SnCl_2$ and the anodic oxide layer was to retard Nb–Sn reaction until a uniform tin film is formed. However, previous studies of the nucleated surface only indicated the

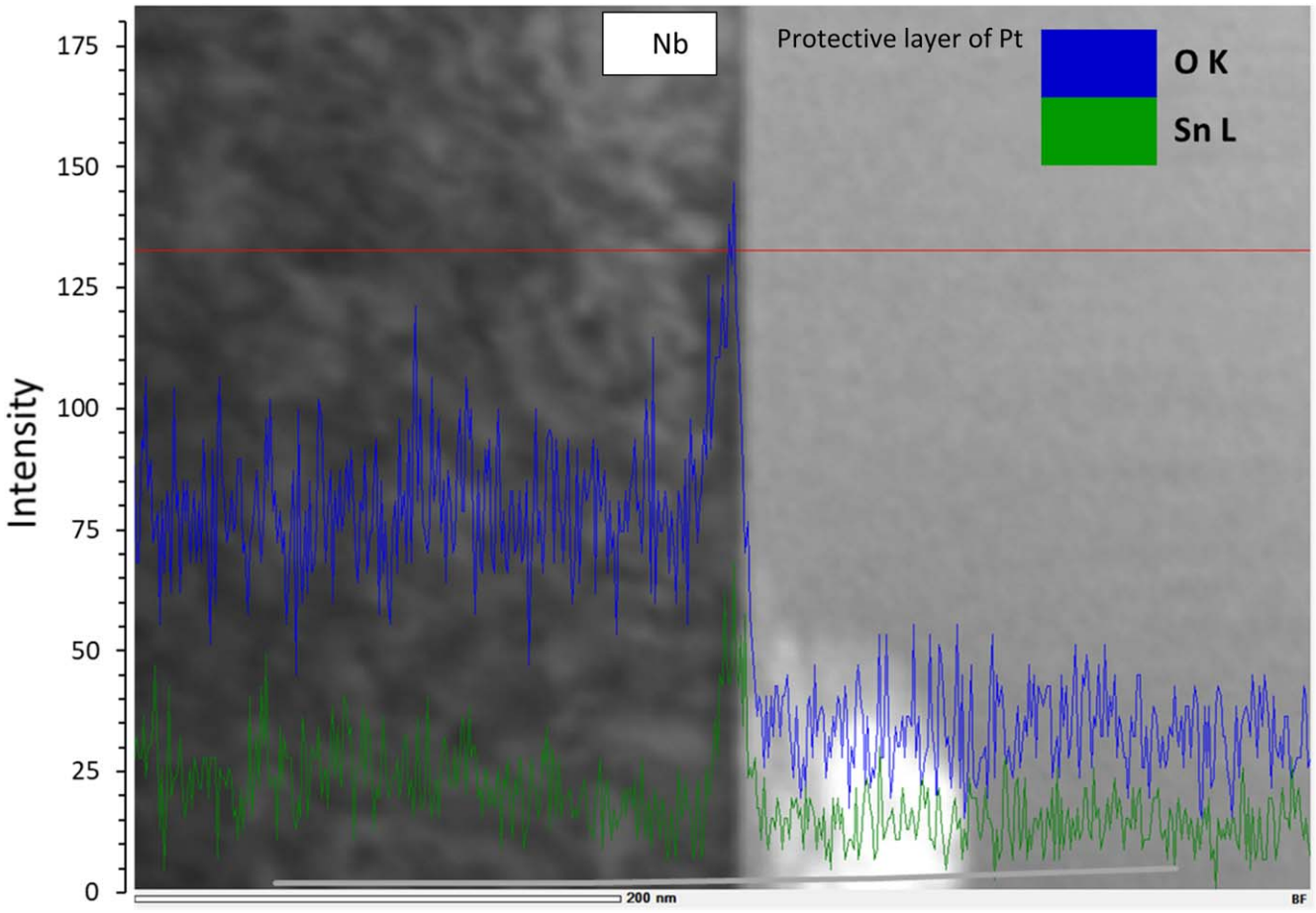


**Figure 7.** TEM cross-section of a sample nucleated at 500 °C for 5 h. EDS spectra from a line scan that follows solid red line is superimposed on top of TEM image. Nb signal is left out to make scaling reasonable for other signals. Note the jump of the Sn and O signal near the surface.

formation of tin particles like in Volmer–Weber mode on the surface following nucleation [15]. The presence of a tin film was not established.

### *3.2. Nucleation time variation at 500 °C*

The nucleation time was varied while keeping the temperature constant at 500 °C. It was found that five minutes at 500 °C was not enough to evaporate all the Sn chloride (1 g), but it was sufficient to produce some Sn particles already. The surface was covered with 'curly' features as shown in figure 9(a). Results obtained after an hour at the same temperature were discussed already in the previous section. The surface produced after four hours at 500 °C is shown in figure 9(b). Comparing with the result obtained after an hour at 500 °C, four hours at same temperature appears to produce additional small Sn particles resulting in more coverage on the surface. EDS was only able to detect Sn from large Sn particles, but once again XPS analysis showed more Sn than SEM/EDS analysis reported. Comparison of XPS analysis is presented in table 7.

The AFM image captured from a sample prepared at the nucleation temperature of 500 °C for 4 h is shown in figure 10(a). Note that the size of the largest tin particle (see height profile of a section at figure 10(b)) is similar at the base when compared to that obtained after an hour at 500 °C (figure 8), but thicker.

### *3.3. Low versus high amount of tin chloride*

The recipe for diffusion coating of $Nb_3Sn$ first developed at Siemens AG used a very small amount of tin halide (20 $\mu$g cm$^{-2}$). Figure 11 shows the result of using still less, reported by Cornell University ($\sim$10 $\mu$g cm$^{-2}$ of tin chloride, 500 °C for five hours, temperature ramp at 3 °C min$^{-1}$) [37]. The SEM image shows a uniform distribution of particles. They are very small compared to those produced with a higher amount of tin chloride. EDS examination showed only Nb indicating that these particles are thin. XPS analysis (table 8) shows tin coverage comparable to that obtained higher loadings Notice that removal of carbon by pre-sputtering revealed significant niobium, but actually reduced the tin, consistent with the notion of a very thin surface layer. Evidently more tin chloride produces bigger tin particles with similar tin coverage on niobium surface. The longer nucleation time in later recipe may have an important role to produce such a good coverage of tin with a small amount of tin chloride.

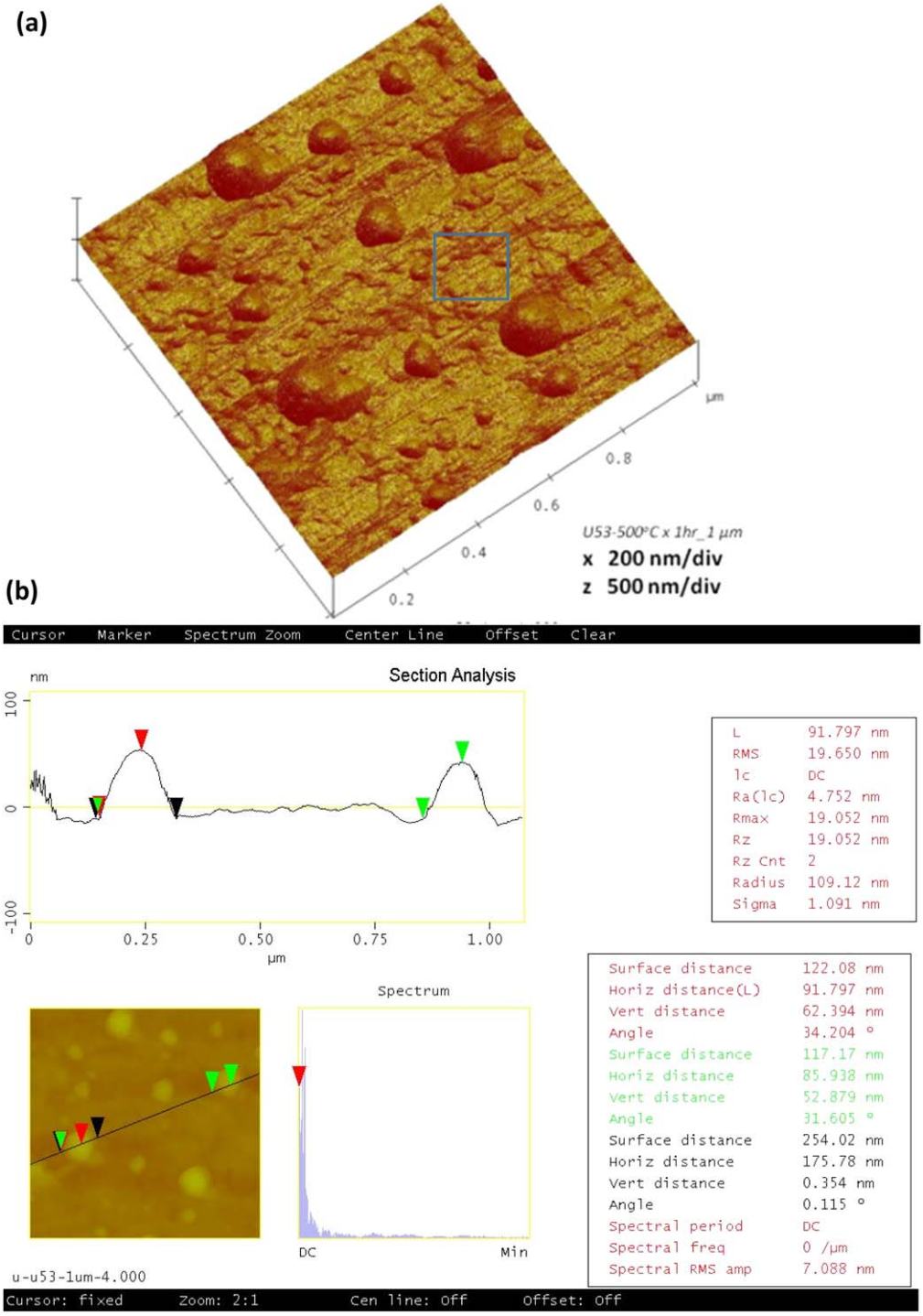


**Figure 8.** AFM image obtained from sample treated at 500 °C for an hour is shown in (a). Note that scan size is only 1 $\mu$m × 1 $\mu$m. Sn particles appear to be three dimensional clusters forming islands. Height profile along the line passing through the tin island is shown in (b). Triangles of the matching color are reference points for the height measurements.

### *3.4. Nucleation on anodized surfaces*

Substrate anodization was introduced in the 1970s to overcome non-uniformity and was often combined with the setup that maintains higher temperature of the tin source compared to the substrate [22]. Despite the expected RRR loss, recent coating experiments with anodized substrates using the 'standard' nucleation protocol indicated a positive effect for the coating uniformity [38, 39]. We compared the effect of tin chloride on nucleation on anodized and non-anodized niobium surfaces. A fixed cell voltage of 30 or 50 V was applied to grow anodic oxide layers on BCP treated Nb samples with 15% $NH_4OH$ solution as an electrolyte. The thickness of the oxide layers was estimated to be 72 nm and 120 nm respectively for the samples using the reported thickness-voltage

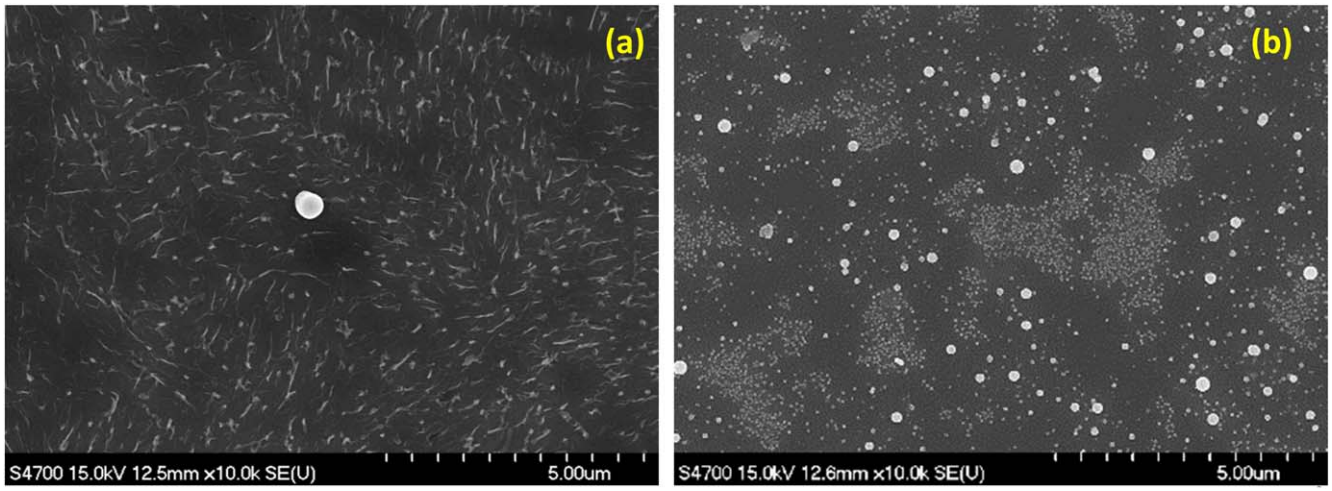


**Figure 9.** SEM images from samples obtained from experiments with nucleation temperature of 500 °C for (a) 5 min and (b) 4 h.

**Table 7.** XPS elemental analysis of nucleated samples for different durations at 500 °C.

| Nucleation temperature (°C) | Time | Sample | C (at%) | O (at%) | Nb (at%) | Sn (at%) | $\frac{Sn}{Nb+Sn} \times 100$ | |
|---|---|---|---|---|---|---|---|---|
| 500 °C | 4 h | U1 | 7.2 | 61.3 | 23.9 | 12.0 | 33.42 | With pre-sputtering |
| 500 | 1 h | U90 | 56.8 | 31.2 | 7.3 | 4.7 | 39.17 | |
| | | | 13.3 | 52.5 | 25.3 | 8.9 | 26.02 | With pre-sputtering |
| 500 °C | 5 min | U9 | 39.9 | 42.0 | 11.9 | 6.2 | 34.25 | |
| | | | 2.4 | 42.7 | 51.3 | 3.6 | 6.55 | With pre-sputtering |

ratio [40]. These samples were subjected to 5 h of nucleation at 500 °C with the usual amount of $Sn/SnCl_2$. SEM images of the obtained surfaces are shown in figure 12. Bright features were present on the surface following nucleation in each sample, but the appearance and distribution of these features (presumably tin) were different from those observed for non-anodized samples. Bright features were bigger and more sparsely distributed in a 50 V anodized sample compared to those in a 30 V anodized sample. Our result appears to be different from recent results from similar studies [41], which report the formation of big tin particles on the surface after preanodization unlike non-anodized Nb. Note that a smaller amount of tin chloride and different anodization parameters compared to our experiments were used in the latter studies.

### *3.5. Variation of tin particle density*

During the course of nucleation studies, the accumulation of visible tin particles seemed to vary for different grains of niobium in some cases as shown in figure 13. The size and shape of tin particles on different niobium grains also varied in this case. Area A1 appears to have fewer particles that appear to be near circular under SEM whereas area A2 seems to have more particles with noncircular shape. Some surface defects in substrate niobium seemed to be a favorable location for particle accumulation in many cases. One example of such defect is a surface scratches, as shown with arrows in figure 13, developed during the polishing of niobium sample. Each scratch line is decorated with a higher density of particles following the nucleation.

### *3.6. $Nb_3Sn$ coatings with different nucleation profiles*

A selected few nucleation profiles were then used for complete $Nb_3Sn$ coating. The temperature profile used during the coating was similar to figure 2 except for the variation in nucleation parameters. There were no evident differences in terms of structure and composition in SEM/EDS between the coatings produced with different nucleation profiles: 400 °C for an hour, 500 °C for an hour and 500 °C for 4 h for similar amount (3 mg $cm^{-2}$) of tin and tin chloride. Obtained SEM images are shown in figure 14, which also includes the coatings produced by applying standard (3 mg $cm^{-2}$) and low (20 $\mu$g $cm^{-2}$) amounts of tin chloride for nucleation.

### *3.7. Role of nucleation in coating genesis*

The coating process with or without tin chloride was interrupted at different times, while following the standard temperature profile as shown in figure 2. The heat was turned off after 1 min, 5 min, 1 h or 3 h. SEM images obtained from each experiment are presented in figures 15 and 16. Five minutes after reaching 1200 °C, a uniform coating with grain size of a few tens of nanometers was developed on the whole niobium surface, when tin chloride was included. Some tin droplets were visible. Similar experiments for one minute at 1200 °C without tin chloride (figure 16) resulted in a coating that included many patchy areas with irregular grain structures. Without tin chloride, these patchy areas appeared both after one hour and the complete coating for 3 h at 1200 °C. On the other hand, coatings obtained from similar experiments with

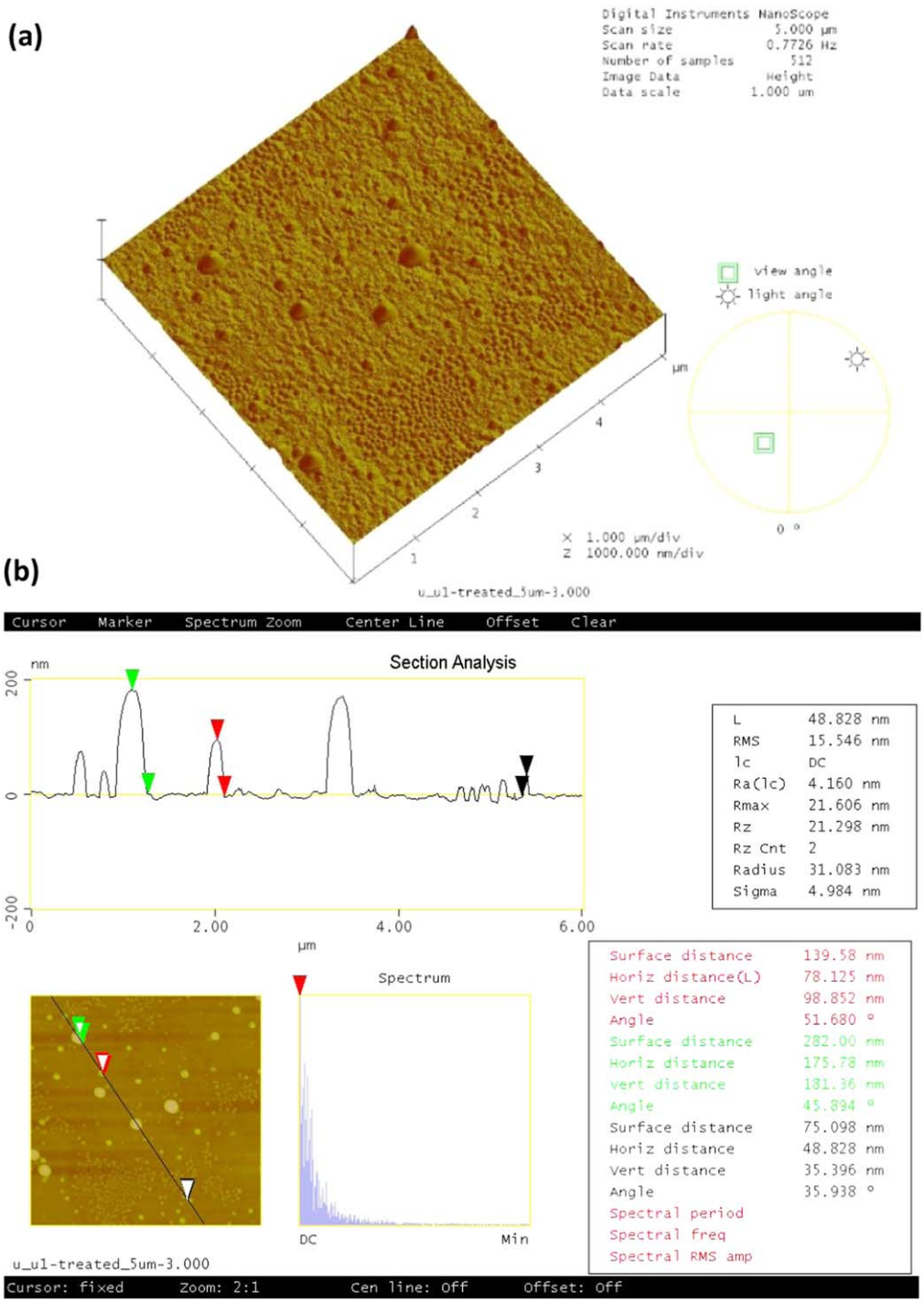


**Figure 10.** AFM image of the surface after 4 h of nucleation at 500 °C is shown in (a). (b) Height profile along a line passing through tin particles. The largest particle is ∼300 nm in diameter with height of ∼175 nm. Triangles of the matching color are reference points for the height measurements.

provided tin chloride demonstrated little to no patchy regions. Repeated complete coating experiments without tin chloride often produced patchy regions with irregular grain structure. This indicated that the inclusion of tin chloride in nucleation step helps to assure a uniform $Nb_3Sn$ coating compared to that without tin chloride. Note that patch-free coatings were also obtained in an experiment without tin chloride. This may have been due to higher tin evaporation rate than normal, since the supplied tin was not packaged in niobium foil, thus providing relatively more surface area for evaporation. Taken together with previous observations, the notion emerges that patch-free coatings are promoted by increased tin supply obtained by tin chloride, more open tin source, or increased tin source temperature (secondary heater).

Finally, we attempted to grow the complete coating without any tin metal, i.e., only $SnCl_2$ was used. The coating

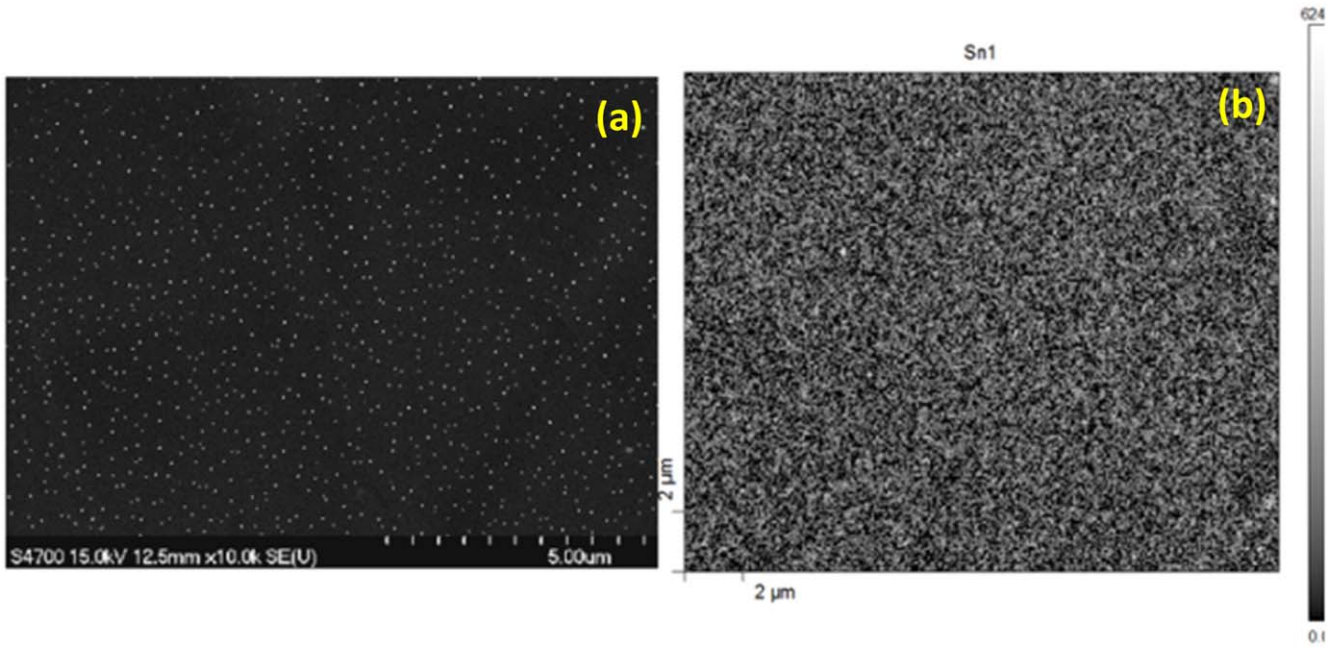


**Figure 11.** (a) SEM image of nucleated surface obtained by using low tin chloride. (b) SAM elemental mapping of tin.

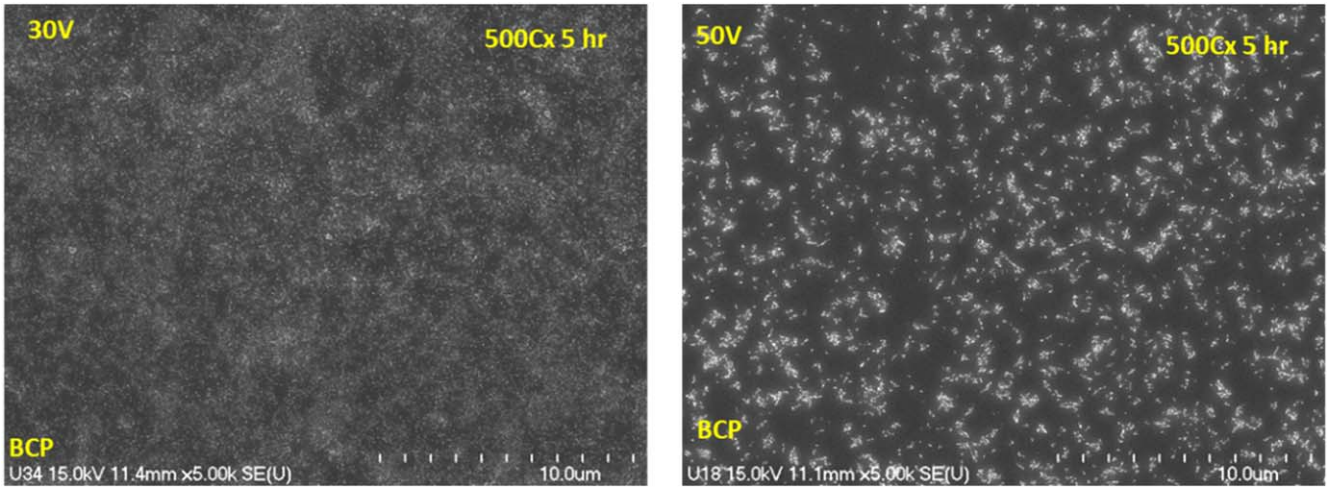


**Figure 12.** Nucleation on niobium anodized at 30 volts (left) or 50 volts (right) to obtain nominal oxide thicknesses of 72 nm or 120 nm, respectively. Processed for 5 h at 500 °C with 3 mg $cm^{-2}$ each of $SnCl_2$ and Sn metal. Particle formation and growth are significantly more evident on the 50 V sample. Compare to non-anodized surface—figure 9.

**Table 8.** XPS elemental analysis of nucleated samples treated for 5 h at 500 °C with reduced amount of $SnCl_2$.

| Nucleation temperature (°C) | Time | Sample | C (at%) | O (at%) | Nb (at%) | Sn (at%) | $\frac{Sn}{Nb+Sn} \times 100$ | |
|---|---|---|---|---|---|---|---|---|
| 500 | 5 h | U66 | 30.5 | 40.7 | 11.1 | 17.7 | 61.45 | |
| | | | 6.0 | 45.5 | 39.7 | 8.8 | 18.1 | With pre-sputtering |

process included nucleation (500 °C for 5 h) and growth (1200 °C for 3 h) with 2 g of tin chloride. A SEM image of the coating is shown in figure 17. Complete coverage of coating was observed with some patchy areas and elongated grains. However, it shows that $SnCl_2$ plays an important role to establish a continuous tin layer prior to tin evaporation during the growth process.

### *3.8. Mechanism of tin deposition via $SnCl_2$*

The native niobium surface is covered by 4–6 nm thick layer of $Nb_2O_5$ [42]. The presence of underlying suboxides ($NbO_2$, NbO, $Nb_2O$, $Nb_2O_3$) was inferred from Nb binding energies observed by XPS [43, 44]. The thermal stability of the native oxide layer has been studied with respect to SRF cavities. These works generally agree that the typical $Nb_2O_5$ layer

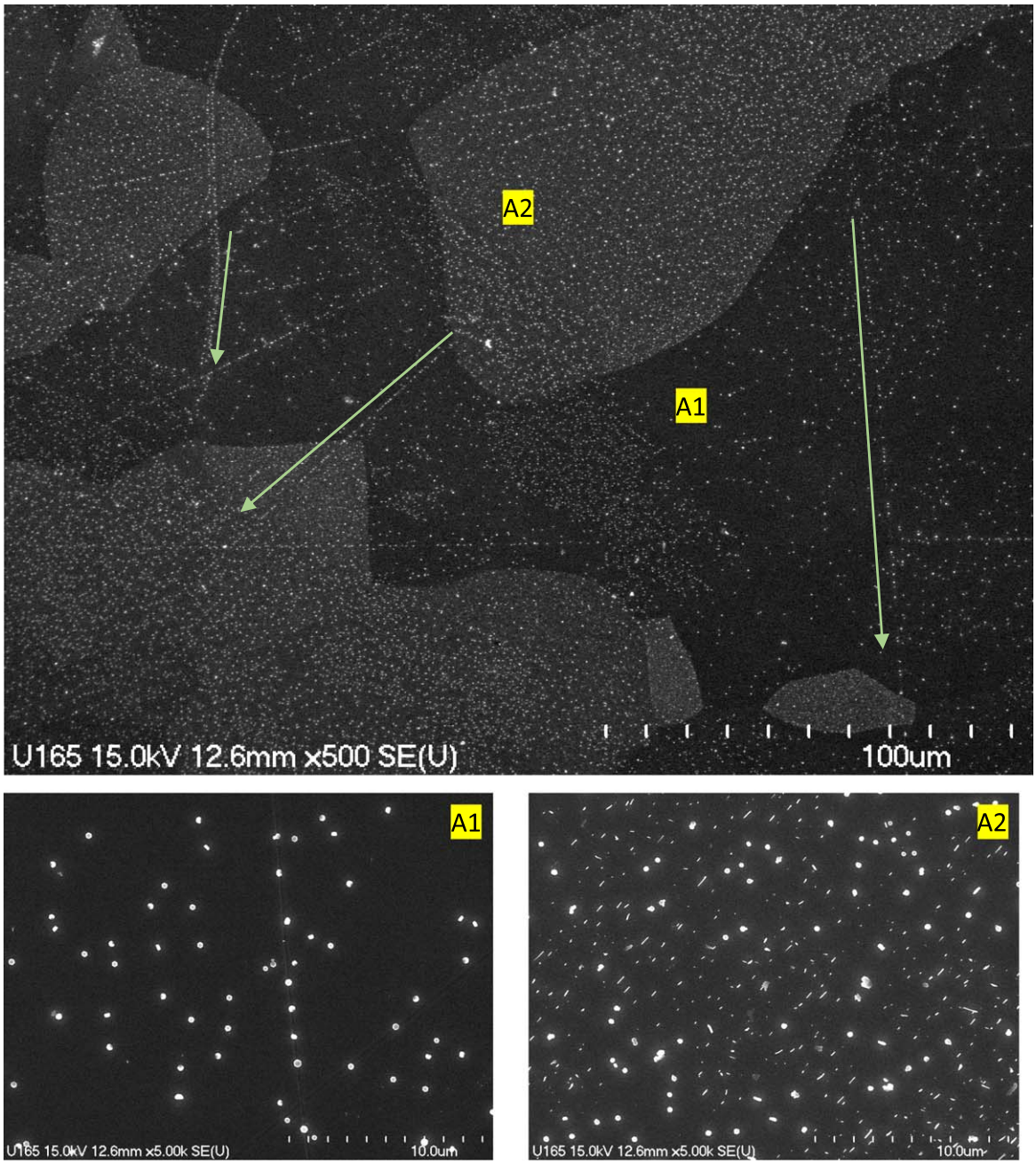


**Figure 13.** Variation of tin particle population in different Nb grains after nucleation at 500 °C for 3 h with 3 mg cm$^{-2}$ each of $SnCl_2$ and Sn metal. In the top image, the letters A1 and A2 indicate the location of two images below. The arrows are closely adjacent and parallel to the now-decorated scratches next to them. In the lower images A1 and A2 evidence different particle distributions.

reduces to $NbO_2$, and then to NbO following UHV baking at temperature >300 °C [43]. The studied nucleation temperatures are in the range where the reduction of native $Nb_2O_5$ layer progresses. Molecular water, hydrogen-bound water and hydroxyl water are expected as well.

During nucleation $SnCl_2$ reacts to deposit tin-rich features and lose chlorine. Three reaction paths may be envisioned. First (a), it may react with some small amount of hydroxyl present in the nucleation chamber. Second (b), interaction with niobium oxide covering the surface may take place, A third (c) possibility is direct reaction between $SnCl_2$ and niobium surface. These reactions may be summarized as

$$SnCl_2 + H_2 \rightarrow Sn + 2HCl \quad \text{(a)}$$

$$3SnCl_2 + 2NbO \rightarrow 2NbOCl_3 + 3Sn \quad \text{(b)}$$

$$x\ SnCl_2 + 2\ Nb \rightarrow 2\ NbCl_x + x\ Sn. \quad \text{(c)}$$

Gibbs free energy data [45] show that reaction (a) happens at ∼1500 °C under standard conditions, but is less favored for nucleation temperatures. On the other hand, reduction of $SnCl_2$ with hydrogen has been reported before to deposit Sn on copper in a similar scenario, where HCl pressure must be kept low [46]. We can expect level of HCl in our

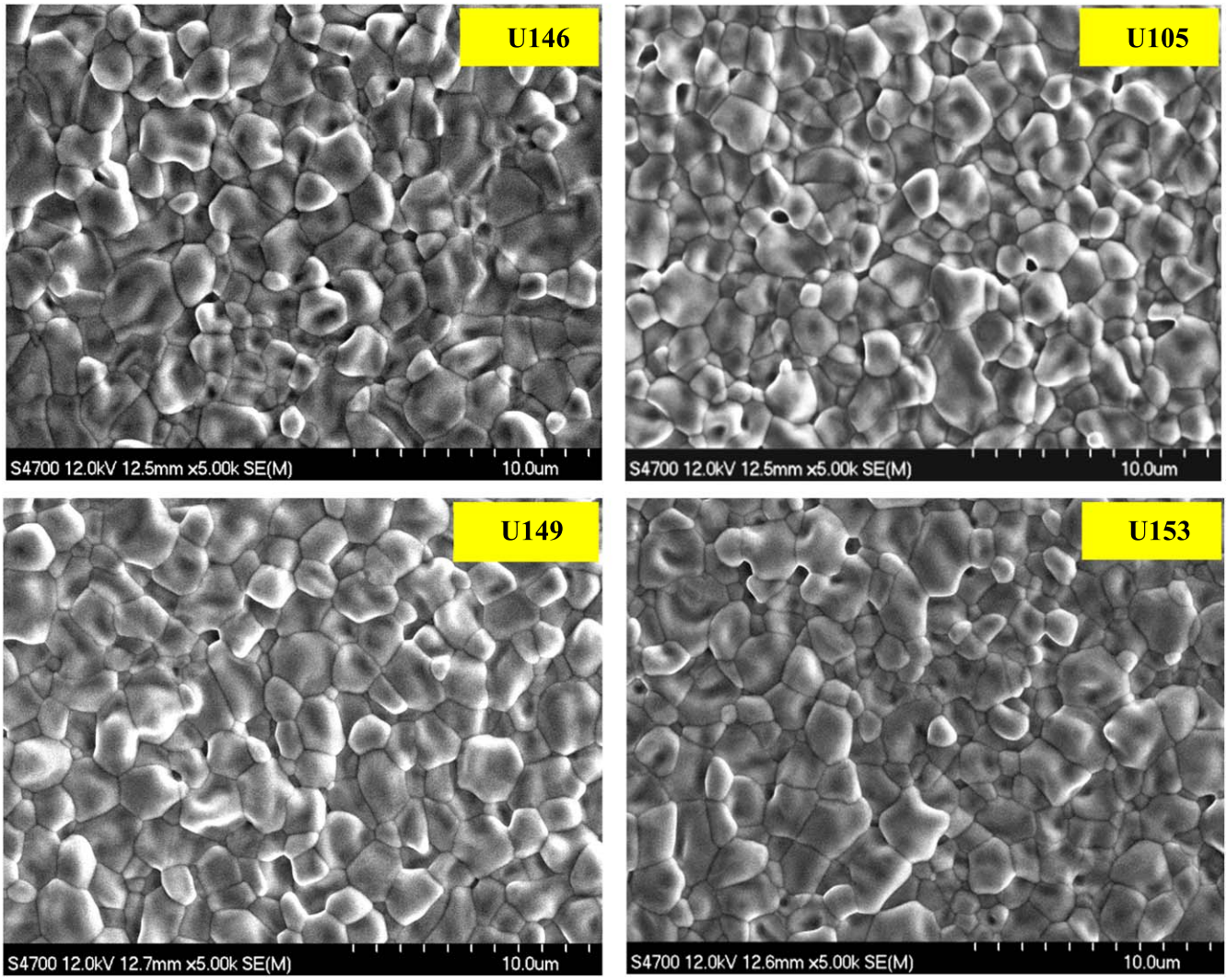


**Figure 14.** $Nb_3Sn$ coatings obtained by applying different nucleation profiles. U146, U105, U149 and U153 involved nucleation step 400 °C × 1 h, 500 °C × 1 h and 500 °C × 4 h and 500 °C × 5 h respectively. U153 was coated with only ∼5 mg of $SnCl_2$, and involved additional coating time of 6.5 h at 1100 °C.

experiment to be low as the insert was constantly pumped during the experiment. Further, both hydrogen and HCl were observed with residual gas analyser (RGA) during some of our nucleation experiments, so this path seems plausible. Since possible chlorination of $Nb_2O_5$ at low temperature through an intermediate step involving the formation of niobium oxychloride has been suggested before [47–49], we consider the possible interaction of $SnCl_2$ with niobium oxide. X-Ray Reflectivity (XRR) studies on Nb (110) claim that $Nb_2O_5$ and $NbO_2$ both reduce to NbO following 30 min of vacuum annealing at 300 °C [50]. So, we only illustrated equation (b) here, but the thermodynamic data are not all available to check its feasibility. In reaction (c), x can be 3, 4 or 5. It is found that $NbCl_3$ is favored the most for any temperature <500 °C compared to $NbCl_4$ under standard condition. $NbCl_5$ is not thermodynamically favored in our experimental temperatures [45]. Besides the possible reactions producing tin, concomitant reduction of niobium oxide layer upon the arrival of $SnCl_2$ vapor, the mobility and surface diffusion of tin, niobium surface properties (e.g. defects, orientation) are other factors to be considered to explain the produced nucleated surfaces from different experiments.

Since the evaporation of $SnCl_2$ is expected to start at ∼250 °C, the known transformation of the native $Nb_2O_5$ surface in this temperature range occurs in its presence. We envision that as we heat the niobium surface, oxide dissolution results in randomly distributed defects first at lower temperature. These sites are favorable to trap tin early. Because of low amount of $SnCl_2$ evaporation at lower temperature (∼300 °C), these particles are only a few nanometers in size. Further heating increases both the defect population and the $SnCl_2$ partial pressure. Such locations enhance $SnCl_2$ interaction with the Nb surface producing more tin, bringing in features shown in figure 4(b) at about 400 °C. Raising nucleation temperature further to (450–500) °C is expected to produce more defects in the oxide layer leading to more particles. The native niobium

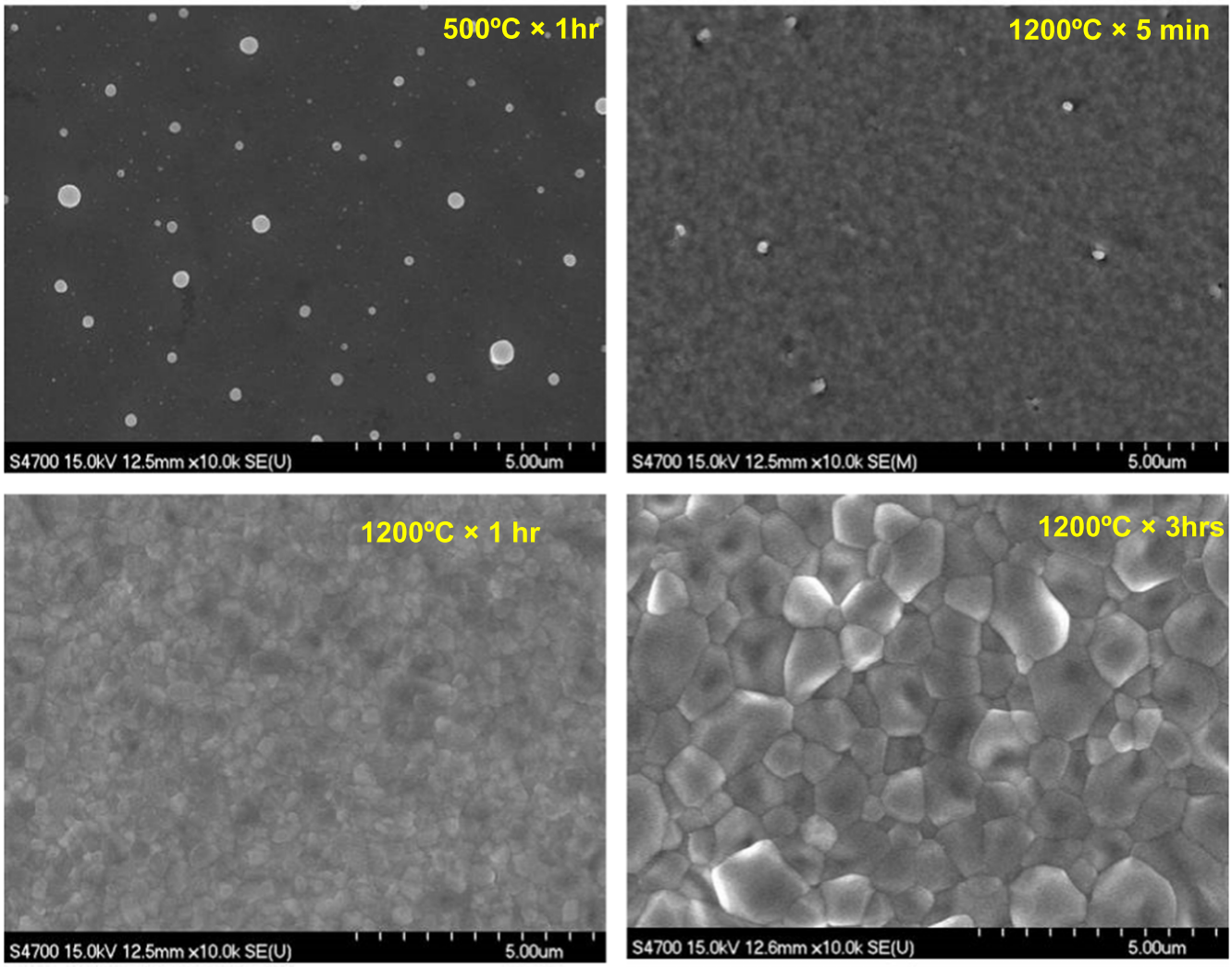


**Figure 15.** Stages of coating growth with tin chloride included. Completion of nucleation (top left), initial coating growth (top right), middle of growth process (bottom left) and growth completion (bottom right). The bigger tin particles are still visible after 5 min at 1200 °C.

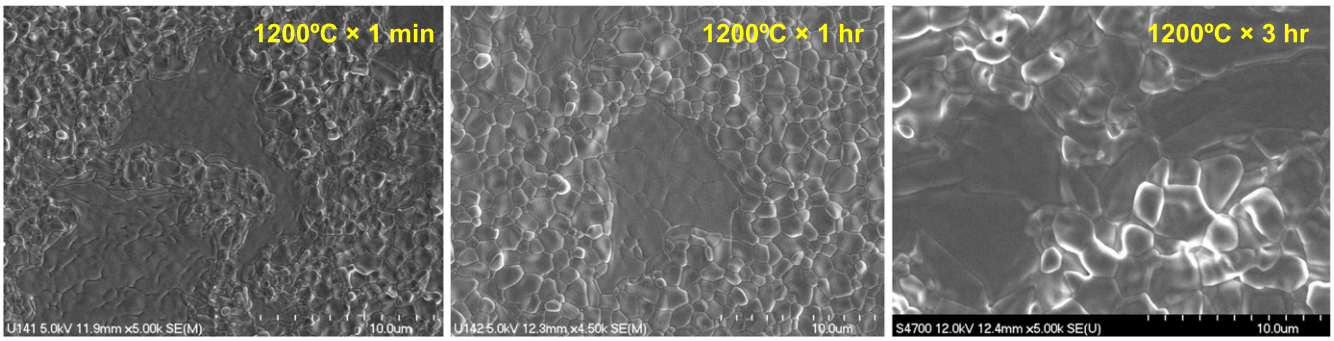


**Figure 16.** Coating growth as in figure 15, but without tin chloride. Coatings obtained after 1 min, 1 h and 3 h at 1200 °C are shown respectively.

oxide layer would have reduced completely after few minutes at these temperatures. A reaction between $SnCl_2$ and niobium may take place uniformly, as suggested by reaction (c) at this point forming tin surface layer by the direct reaction between $SnCl_2$ and Nb. Longer nucleation may add further tin to the thin film and particles. The equilibrium surface composition is determined by tin arrival as well as tin–tin and tin–surface interaction.

Surface defects, like the scratch discussed here have different surface diffusion rates from flat surface [51]. Sn atoms bond more favorably to these less coordinated sites, and they serve as sinks for Sn during Sn vapor deposition

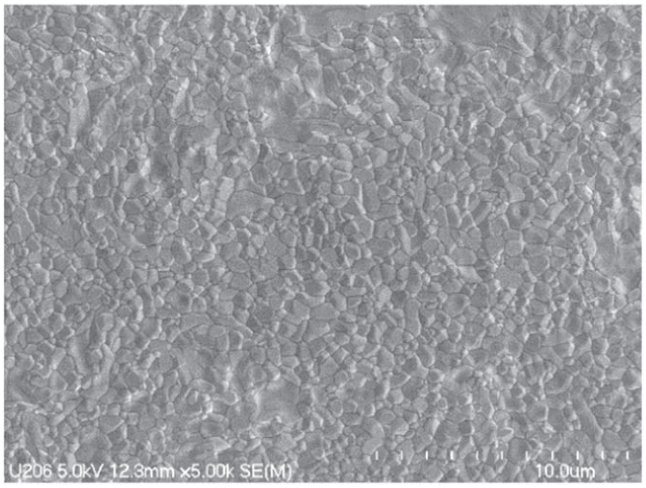


**Figure 17.** Complete coating prepared with only $SnCl_2$. in both steps; no tin metal was used. A substantially complete coverage of coating was obtained, though with some irregular grain structures and patches.

favoring the formation of tin particles. The different density of particles on different grains raises the question an orientation-dependent adatom-surface interaction. One can expect the anisotropy in tin adsorption because of anisotropic surface energy. For example Nb(110) has the lowest surface energy because of bcc structure [52].

## 4. Conclusions

Advanced materials characterization tools, notably XPSy and SAM, revealed useful new information as well as raising questions of uniformity and distribution.

Nucleation yields two tin forms. At all loadings, a two-dimensional form no thicker than a few atom layers is evident to surface spectroscopies and analytical TEM. Especially at higher loadings, three-dimension particles are quite visible to scanning electron microscopy and atomic force microscopy.

The inclusion of tin chloride in any explored nucleation profile appeared advantageous toward producing a defect free $Nb_3Sn$ coating compared to the same coating obtained without it.

Even though the variation of nucleation parameters was able to produce drastically different surface appearance, no evidence of any significant impact on the final coating within a considerable parameter range was found with SEM/EDS.

## Acknowledgments

Thanks to Olga Trifimova for her help with AFM. SAM measurement was done at Swagelok Center for Surface Analysis of Materials at Case Western Reserve University. Work at College of William & Mary was supported by Office of High Energy Physics under grant SC0014475. Partially authored by Jefferson Science Associates under contract no. DEAC0506OR23177.

## ORCID iDs

Michael J Kelley https://orcid.org/0000-0003-0621-5005

## References

[1] Padamsee H, Knobloch J and Hays T 1998 *RF Superconductivity for Particle Accelerators* (New York: Wiley)
[2] Matthias B T, Geballe T H, Geller S and Corenzwit E 1954 Superconductivity of $Nb_3Sn$ *Phys. Rev.* **95** 1435
[3] Transtrum M K, Catelani G and Sethna J P 2011 Superheating field of superconductors within Ginzburg–Landau theory *Phys. Rev.* B **83** 094505
[4] Dickey J M, Strongin M and Kammerer O F 1971 Studies of thin films of $Nb_3Sn$ on Nb *J. Appl. Phys.* **42** 5808–20
[5] Rossi A A, Deambrosis S M, Stark S, Rampazzo V, Rupp V, Sharma R G, Stivanello F and Palmieri V 2009 $Nb_3Sn$ films by multilayer sputtering *Proc. SRF 2009 (Berlin, Germany)*
[6] Deambrosis S M, Keppel G, Ramazzo V, Roncolato C, Sharma R G and Palmieri V 2006 A15 superconductors: an alternative to niobium for RF cavities *Physica* C **441** 108–13
[7] Mitsunobu S 2010 Status of KEK studies on $MgB_2$ *Proc. 4th Int. Workshop on Thin Films and New Ideas for Pushing the Limits of RF Superconductivity (Padua, Italy)*
[8] Rosaz G J, Calatroni S, Leaux F M, Motschmann F, Mydlarz Z, Taborelli M and Vollenberg W 2015 Development of $Nb_3Sn$ coatings by magnetron sputtering for SRF cavities *Proc. 17th International Conference on RF Superconductivity (Whistler, BC, Canada)* pp 691–4 TUPB051
[9] Krishnan M, James C and Bures B 2012 Energetic condensation growth of $Nb_3Sn$, MoRe and $MgB_2$ films for SRF accelerators *5th Int. Workshop on Thin Films Applied to Superconducting RF and New Ideas for Pushing the Limits of RF Superconductivity (Newport News, VA, USA)*
[10] Barzi E, Bestetti M, Reginato F, Turrioni D and Franz S 2015 Synthesis of superconducting $Nb_3Sn$ coatings on Nb substrates *Supercond. Sci. Technol.* **29** 015009
[11] Neugebauer C A 1964 Thin films of niobium tin by codeposition *J. Appl. Phys.* **35** 3599–603
[12] Saur E and Wurm J 1962 Präparation und Supraleitungseigenschaften von Niobdrahtproben mit $Nb_3Sn$-Überzug *Naturwissenschaften* **49** 127–8
[13] Arnolds G and Proch D 1977 Measurement on a $Nb_3Sn$ structure for linear accelerator application *IEEE Trans. Magn.* **13** 500–3
[14] Kneisel P, Stoltz O and Halbritter J 1979 Measurements of superconducting $Nb_3Sn$ cavities in the GHz range *IEEE Trans. Magn.* **15** 21–4
[15] Müller G, Roeth R, Piel H, Mansen D, Pouryamout J and Kneisel P 1996 $Nb_3Sn$ layers on high purity Nb cavities with very high quality factors and accelerating gradients *EPAC 1996 (Barcelona, Spain)* pp 208–2087
[16] Liepe M and Posen S 2013 $Nb_3Sn$ for SRF application *Proc. 16th Int. Conf. on RF Superconductivity (Paris, France, 23–27 September)* pp 773–6 WEIOA04
[17] Posen S, Romanenko A, Merio M and Trenikhina Y 2015 Fermilab $Nb_3Sn$ R&D program *Proc. 17th Int. Conf. on RF Superconductivity (Whistler, BC, Canada, 13–18 September )* pp 678–80 TUPB048
[18] Eremeev G V, Clemens W A, Macha K, Park H and Williams R S 2013 Commissioning results of $Nb_3Sn$ cavity vapor diffusion deposition system at JLab *Proc. 6th Int. Particle Accelerator Conf. (Richmond, VA, USA, 2013)* pp 3512–4 WEPWI011

[19] Posen S, Liepe M and Hall D L 2015 Proof-of-principle demonstration of $Nb_3Sn$ superconducting radiofrequency cavities for high $Q_o$ applications *Appl. Phys. Lett.* **106** 082601
[20] Posen S and Hall D L 2017 $Nb_3Sn$ superconducting radiofrequency cavities: fabrication, results, properties, and prospects *Supercond. Sci. Technol.* **30** 033004
[21] Charlesworth J P, Macphail I and Madsen P E 1970 Experimental work on the niobium-tin constitution diagram and related studies *J. Mater. Sci.* **5** 580–603
[22] Hillenbrand B, Martens H, Pfister H, Schnitzke K and Uzel Y 1977 Superconducting $Nb_3Sn$ cavities with high microwave qualities *IEEE Trans. Magn.* **13** 491–5
[23] Wilhelm M, Frohmader S and Ziegler G 1976 Herstellung von $V_3Ga$-und $Nb_3Sn$-multifilamentleitern hoher stromtragfähigkeit mit hilfe chemischer transportreaktionen *Mater. Res. Bull.* **11** 491–5
[24] Kneisel P 2012 History of $Nb_3Sn$ developments for superconducting RF Cavities—a review *JLab Technical Note* TN12–016
[25] Band 46 Sn [B] *Gmelins Handbuch der Anorganischen Chemie* (Weinheim: Verlag Chemie) p 176
[26] Band 49 Nb [A] *Gmelins Handbuch der Anorganischen Chemie* (Weinheim: Verlag Chemie) p 234
[27] Landolt-Boernstein Auflage 6, Band II, Teil2, Bandteil:a *Zahlenwerte und Funktionen aus Physik, Chemie, Astronomie, Geophysik und Technik*
[28] Peiniger M, Hein M, Klein N, Müller G, Piel H and Thuenus P 1988 Work on $Nb_3Sn$ cavities at Wuppertal ANL-PHY–88-1-VOL 2
[29] Pudasaini U, Kelley M, Eremeev G and Reece C 2015 Local composition and topography of $Nb_3Sn$ diffusion coatings on niobium *17th Int. Conf. on RF Superconductivity (SRF 2015) (Whistler, BC, Canada, 13–18 September 2015)* pp 703–7
[30] Pudasaini U, Eremeev G, Kelley M and Reece C 2017 Experimental study of nucleation for $Nb_3Sn$ diffusion coatings on niobium SRF cavities *28th Linear Accelerator Conf. (LINAC'16) (East Lansing, MI, USA, 25–30 September 2016)* pp 740–3
[31] Vickerman J C and Gilmore I S (ed) 2011 *Surface Analysis: The Principal Techniques* (New York: Wiley)
[32] Hesse R, Streubel P and Szargan R 2005 Improved accuracy of quantitative XPS analysis using predetermined spectrometer transmission functions with UNIFIT 2004 *Surf. Interface Anal.* **37** 589–607
[33] Powell C J and Jablonski A 2000 NIST Electron Inelastic-Mean-Free-Path Database 71, Version 1.1 (NIST NSRDS)
[34] Wu Z and Dickey J M 2000 Growth mode of tin on a niobium substrate *Thin Solid Films* **371** 161–6
[35] Eisenmenger-Sittner C, Bangert H, Störi H, Brenner J and Barna P B 2001 Stranski–Krastanov growth of Sn on a polycrystalline Al film surface initiated by the wetting of Al by Sn *Surf. Sci.* **489** 161–8
[36] Hillenbrand B 1980 The preparation of superconducting $Nb_3Sn$ surfaces for RF applications *Proc. 1st Workshop on RF Superconductivity (KFK, Karlsruhe)*
[37] Posen S 2015 Understanding and overcoming limitation mechanisms in $Nb_3Sn$ superconducting RF cavities *PhD Thesis* Cornell University
[38] Pudasaini U, Eremeev G, Kelley M, Reece C and Tuggle J 2018 Surface studies of $Nb_3Sn$ coated samples prepared under different coating conditions *18th Int. Conf. on RF Superconductivity (SRF'17) (Lanzhou, China, 17–21 July 2017)* pp 894–9
[39] Hall D L, Liepe M, Porter R D, Arias T, Cueva P, Liarte D B, Muller D A, Sethna J P and Sitaraman N 2018 High performance $Nb_3Sn$ cavities *18th Int. Conf. on RF Superconductivity (SRF'17) (Lanzhou, China, 17–21 July 2017)* pp 667–73
[40] Kneisel P 1980 Surface preparation of niobium *Proc. 1st Workshop on RF Superconductivity (KFK, Karlsruhe)* pp 27–40
[41] Hall D L 2017 New insights into the limitations on the efficiency and achievable gradients in $Nb_3Sn$ SRF cavities *PhD Thesis* Cornell University
[42] Tian H, Reece C E, Kelley M J, Wang S, Plucinski L, Smith K E and Nowell M M 2006 Surface studies of niobium chemically polished under conditions for superconducting radio frequency (SRF) cavity production *Appl. Surf. Sci.* **253** 1236–42
[43] King B R, Patel H C, Gulino D A and Tatarchuk B J 1990 Kinetic measurements of oxygen dissolution into niobium substrates: *in situ* x-ray photoelectron spectroscopy studies *Thin Solid Films* **192** 351–69
[44] Ma Q and Rosenberg R A 2003 Angle-resolved x-ray photoelectron spectroscopy study of the oxides on Nb surfaces for superconducting rf cavity applications *Appl. Surf. Sci.* **206** 209–17
[45] Yorucu H and Sale F R 1982 The production of niobium-tin powders by vapor-deposition processes *Metall. Trans.* B **13** 625–31
[46] Brear J M and Sale F R 1974 The vapour phase stannising of copper *J. Less Common Metals* **38** 221–32
[47] Gaballah I and Djona M 1994 Processing of spent hydrorefining catalysts by selective chlorination *Metall. Mater.Trans.* B **25** 481–90
[48] Gilchrist J D 1980 Extraction metallurgy *Int. Ser. Mater. Sci. Technol.* (London: Pergamon)
[49] Gonzalez J, Gennari F, Bohé A, Ruiz M D C, Rivarola J and Pasquevich D M 1998 Chlorination of niobium and tantalum ore *Thermochimica Acta* **311** 61–9
[50] Delheusy M 2008 X-ray investigation of Nb/O interfaces *PhD dissertation* Université Paris
[51] Wadley H N G, Zhou X, Johnson R A and Neurock M 2001 Mechanisms, models and methods of vapor deposition *Prog. Mater. Sci.* **46** 329–77
[52] Fellinger M R, Park H and Wilkins J W 2010 Force-matched embedded-atom method potential for niobium *Phys. Rev.* B **81** 144119